

Available online at www.sciencedirect.com

ScienceDirect

journal homepage: www.keaipublishing.com/foar



Research Article

Analyzing capacity of a consumer-grade infrared camera in South Africa for cost-effective aerial inspection of building envelopes



Naadir Vorajee a, Asit Kumar Mishra b,*, Amit Kumar Mishra a

Received 24 September 2019; received in revised form 2 May 2020; accepted 14 May 2020

KEYWORDS

IR thermography; Building envelopes; Cost-effective; Thermal images; Image processing; Segmentation algorithms Abstract Prohibitive equipment cost and certain export regulations are the major obstacles to the widespread adoption of infrared (IR) thermography when evaluating building envelopes. In this work, we propose the use of an affordable and easily available camera as a first step of making the technology accessible. Combined with image post-processing, we hypothesize that a low-cost, low-resolution, and consumer-grade device can provide an economic alternative for the periodic evaluation of building envelopes. Following a market survey, the Seek Thermal Compact (STC) was chosen for evaluation. The STC was able to accurately measure the temperature of surfaces and distinguish small thermal anomalies (3 mm in diameter), and the IR images can be post-processed to reasonably estimate the anomaly areas. The STC was particularly effective when images were taken within 1.75 m from the surface. The 1.75 m distance did not pose a challenge in this study, as the goal was to mount the selected IR camera on an unmanned aerial vehicle for the surveys. The small size and weight of the STC were also useful. The results from the analysis of the capability of the STC and the image post-processing techniques may help form the basis of future investigations aiming at lowering the cost of building thermographic surveys.

© 2020 Higher Education Press Limited Company. Production and hosting by Elsevier B.V. on behalf of KeAi. This is an open access article under the CC BY-NC-ND license (http://creativecommons.org/licenses/by-nc-nd/4.0/).

E-mail address: writeto.asit@gmail.com (A.K. Mishra). Peer review under responsibility of Southeast University.

^a Electrical Engineering Department, University of Cape Town, Cape Town 7700, South Africa

^b Berkeley Education Alliance for Research in Singapore, CREATE Tower, 138602, Singapore

^{*} Corresponding author.

1. Introduction

Nearly a third of global final energy consumption (Cox, 2016) and emissions (UNEP, 2012) can be attributed to the built environment. At the same time, the building construction sector accounts for 10% of global gross domestic product (GDP) and provides employment to over 100 million workers (Sun et al., 2016). With growing concerns of a looming energy crisis, climate change, and the need to move towards a sustainable future, the issue of optimal energy use in buildings has become a subject of considerable concern and extensive investigation. Improvements in building energy consumption can be sustained by setting building performance standards and labeling of buildings as the norm (Young et al., 2014). The effective implementation of such standards during design and operation have been shown to aid the goals of energy conservation, cost savings for end users, and emissions reduction (Cox, 2016; Athalye et al., 2016).

About a third of building energy use is directed towards indoor heating and cooling needs (LaFrance et al., 2013). A building's envelope modulates its interaction with the outdoor environment and helps in maintaining livable indoor conditions. The envelope thus plays an essential role in the buildings' overall energy performance. Certain building energy codes can serve as guide in the material selection, effective insulation, and performance and in-use of building envelopes (Kim and Moon, 2009; LaFrance et al., 2013). However, in-use buildings sometimes diverge from their predicted performance (De Wilde, 2014). As a means of overcoming this problem and in ensuring appropriate and timely maintenance, further indicating the in-use compliance to building energy codes, regular inspections are needed by these structures, including building envelopes. However, inspections can become prohibitively costly in terms of human and analytical resources, considering the expanse of a building's envelope.

As code compliance has become increasingly important, regular maintenance to help eliminate subpar energy and/ or comfort-related performance has also become necessary. The demand is both consistent in terms of supporting building inspection and reducing the required time and cost. To this end, the thermal infrared (IR) inspection of buildings has been proposed as a useful tool. IR thermography has been used in building diagnostics for nearly four decades now. IR wavelengths may be classified into the following five bands: near IR, short-wave IR, mid-wave IR (MWIR), long-wave IR (LWIR), and far-infrared IR (Sfarra et al., 2019). MWIR (3-5 μ m) and LWIR (7.5-14.5 μ m) are predominantly used in building diagnostics, as these IR types are less susceptible to atmospheric absorption and more sensitive to objects at ambient temperature, than the other IR types (Balaras and Argiriou, 2002; Avdelidis and Moropoulou, 2003; Kirimtat and Krejcar, 2018). The process of IR thermography is nondestructive and noncontact and can quickly inspect a wide area. Thermographic cameras detect IR radiation and convert it to electrical signal, which is then interpreted into an image representing the radiation intensity.

IR thermography has been successfully used in evaluating building envelope insulation (Ferrarini et al., 2016;

O'Grady et al., 2017; Tejedor et al., 2017) and thermal bridges (O'Grady et al., 2018; Sfarra et al., 2019), estimating building infiltration and leakage (Barreira et al., 2017; Liu et al., 2018), and even understanding how people perceive the performance of their homes (Goodhew et al., 2009). The number of studies involving IR cameras for the evaluation of building performance has consistently increased in recent years (Kirimtat and Krejcar, 2018). The past studies were either dedicated to a specific nature of defect in the building envelope (O'Grady et al., 2018; Liu et al., 2018; Gillott et al., 2016) or as generic as spotting envelope defects (Lagüela et al., 2012; Fox et al., 2016). The studies were either carried out in laboratory conditions (Choi et al., 2007) or at the location of a building (Liu et al., 2018; Nardi et al., 2014). Similar studies may provide a simple qualitative evaluation or strive for a thorough qualitative and quantitative result. The studies that attempted to provide quantitative evaluations mostly used IR imaging combined with the numerical simulation of heat transfer of building elements (Nardi et al., 2014; Lagüela et al., 2012). In the same vein as using numerical techniques combined with IR images, applying image processing techniques to IR images can improve the recognition of temperature contrasts (Kirimtat and Krejcar, 2018). However, to the best of our knowledge, this option has not vet been explored. This approach can particularly benefit the effectiveness of low-cost IR cameras.

The use of IR thermography in investigating the built environment was further developed when unmanned aerial vehicles (UAVs) were brought into the domain. UAVs gradually became cheaper and economically viable for use in building inspections. UAV-mounted IR imaging systems provide greater versatility and are faster than the previous tools, can hover over difficult-to-reach spaces, and can reduce human labor.

The effectiveness of detecting anomalies depends on the quality of the imaging system. Systems with high quality imaging sensors remain prohibitively costly, thus preventing their wide adoption. The current work is targeted at addressing this limitation. We hypothesize that for the drone-mounted inspection of buildings, the use of a lower-sensitivity imaging system, coupled with image post-processing techniques, can provide a viable alternative for the inspection of building envelopes.

This work contributes to the conceptual design of an inexpensive system that uses a low-cost IR camera for the inspection of building envelopes. We present the required process, followed by a discussion of the IR camera used in the current study. Then, an in-depth examination of the performance of the IR camera, along with comparisons with an expensive IR camera, is presented. Another important contribution of this work is the examination of image processing algorithms to substantially bolster the quality of IR images obtained from such an economic device, further aiding the detection of anomalies. Our ultimate goal is to provide a basis for a widespread adoption of thermography in the survey of buildings by providing a viable and economic option to users.

The rest of the paper is organized as follows. Section 2 details the steps in the selection of an appropriate camera, the possible considerations in matching this camera

with a UAV, and the tests to be conducted to validate the IR camera's performance. Section 3 provides the results generated from examining the selected IR camera's performance and discusses their implications. Section 4 presents the conclusions of the study.

2. Methods

In Sections 2.1 to 2.3, we identify the goals of this work and detail the steps in selecting the IR camera. In Section 2.4, we provide a brief list of the steps taken to test the performance of the chosen IR camera. In Section 2.5, we provide the data, the methods for image analysis, and the platforms used.

2.1. Conception goals

The goal of the task was to determine a suitable low-cost IR camera that could be mounted on a low cost UAV. The budget for the camera-UAV combination was set to 10,000 Rands. The UAV, despite its low cost, should have the option to be operated by a control panel or a smart device. The operator would stand at the base of the building. The combination could then be used to remotely survey buildings of any shape and expanse. The UAV should be able to fly with the weight of the camera and other necessary attachments and survey a building within its battery life given a specific flight plan. Due to the limited time allocated for the project, the system setup for combining the UAV and the IR camera was not completed. Instead, with the aim of improving effectiveness, we focused on the selection of an available properly sized IR camera that was appropriately priced and the evaluation and refining of its images through post-processing.

2.2. Selection of an IR camera

IR cameras are not a new technology. However, cost and regulation continue to limit their usability. Hence, an appropriate IR camera needed to be chosen in this study. Different factors, such as cost, availability, resolution, and temperature range, were taken into account when we decided on a viable option. In this paper, when we mention a consumer-grade device, we mean one that is available in most markets worldwide without restrictions. Such a device

should be comparable in cost and frequency of use as everyday electronics, e.g., an average smartphone.

Certain capabilities of the camera itself were considered in this work. For instance, a higher detector resolution allows the visualization of finer details and the attainment of sharper contrasts. The accuracy and sensitivity of the imaging systems were also important considerations in this study. Thermal range describes the maximum and minimum temperatures that a camera can accurately measure. The range varies considerably depending on the model. Span is the difference between the high and low temperature settings in a specific frame's display. The span function can be set as narrow as possible in order for the thermal image to be accentuated and subsequently portray as much detail as possible (Plowright, 2016). The distance between the camera and the envelope and the angle of view can also affect image quality. Owing to the nature of thermal radiation, which can be either be diffused or specular, the viewing angle was of utmost importance in our study. Viewing the targets at an angle perpendicular to the surface was also regarded an ideal scenario.

Table 1 lists the IR cameras explored in this study. The specifications of the different thermal cameras listed in this table do not give a user an intuitive feel of the actual size to be represented by a viewed image. Equation (1) can be obtained using the field of view angle together with the pixel resolution. The equation may then be used to calculate the actual image to be represented by 1 pixel of a chosen thermal camera at a defined distance from target (i.e., operational diameter). Moreover, the equation considers the following properties of the cameras: operational diameter (OD), horizontal field of view (HFOV), and vertical field of view (VFOV). These functions can help users approximate the type of detail to be derived from an image. Equation (1) is further depicted as Fig. 1 in this study.

Area per pixel =
$$\frac{40D^2(tan(0.5HFOV^\circ) \times tan(0.5VFOV^\circ))}{Sensor Resolution} \quad (1)$$

In Equation (1), OD is measured in m, HFOV and VFOV are both measured in degrees, and the sensor resolution is stated in pixels. The area per pixel (APP) for each device is also shown in Table 1, while the values for the three different operational diameters are presented in Table 2. The device with the smallest APP will likely provide the most details per pixel and thus can be regarded as the most useful for the inspection of building envelopes.

Table 1 Specifications of thermal cameras examined in the present study. FOV is the field of view. Prices are given in South African Rands.

Name	Resolution	Temp.Range	Connection	FOV	Price
AMG8833	8 × 8	0:80	I2C	60° × 60°	500
HT-02 (handheld)	60 × 60	-20:300	SD card	$20^{\circ} \times 20^{\circ}$	2250
Seek Thermal	206 × 156	-40:330	micro-USB	$36^{\circ} \times 36^{\circ}$	2500
FLIR Lepton 3 (chip)	160 × 120	-10:65	SPi	$56^{\circ} \times 71^{\circ}$	2900
FLIR 1	80 × 60	-20:120	micro-USB	$50^{\circ} \times 38^{\circ}$	4200
FLIR 1 Pro	160 × 120	-20:400	micro-USB	$50^{\circ} \times 38^{\circ}$	7100
FLIR DUO	160 × 120	-20:60	HDMI	57° × 44°	14,000
Yuneec Typhoon	198 × 128	-10:180	USB	$115^{\circ} \times 115^{\circ}$	21,650
FLIR VUE	336 × 256	-20:50	_	$25^{\circ} \times 19^{\circ}$	25,000
Zenmuse XT	640 × 512	-10:40	micro-SD	90° × 69°	122,560

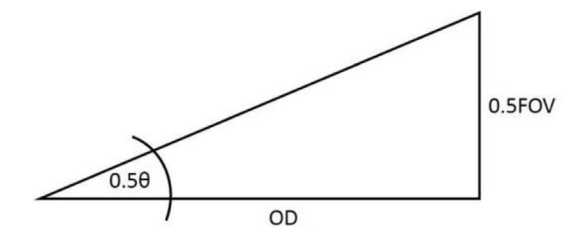


Fig. 1 Geometric interpretation of Equation (1).

FLIR 1 Pro utilizes the Lepton 3 chip together with its proprietary software, resulting in a higher price. FLIR 1 utilizes the Lepton 2 chip and a filtering software, thus providing a clearer IR image. Although FLIR 1 has a larger APP value than Seek Thermal, its filtering software takes the IR image and an optical image of the same object and then passes the optical image through a high pass filter to obtain the outlines of the target object. The result is an overall better appearance of images from FLIR 1 than those of Seek Thermal. Here, FLIR Lepton (3 or 2) is simply considered a camera module; that is, the IR sensor chip is the main advantage but not the camera itself.

FLIR VUE has the smallest APP value (0.4 at 5 m), followed by Zenmuse XT. However, both cameras are prohibitively expensive. FLIR DUO is expensive, but its APP values are more in line with our work than the other analyzed camera models. Thus, our selection.

Focused on Seek Thermal, FLIR Lepton 3, or FLIR 1. Even with a larger APP value, FLIR 1 can produce better defined images than Seek Thermal. However, apart from the budgetary constraints, another hurdle we encountered was the export regulations, in which FLIR cameras cannot be easily obtained in many countries around the world. A

possible reason is that FLIR Lepton camera modules are also used as military equipment. Such regulations contribute to the low adoption of IR cameras. Hence, we proceeded with the purchase of Seek Thermal, which has an APP of 3.1 at an operational diameter of 5 m. However, only the compact version of Seek Thermal can be shipped to South Africa. Seek Thermal Compact (STC) has a dimension of 2.54 cm \times 4.45 cm \times 2.03 cm and a mass of 14.17 g (Seek Thermal). The STC can be interfaced with a smartphone for the recording of IR images.

2.3. Selection criteria for a suitable UAV

The UAV should be able to hover flight, operate in a confined area, be used easily, and offer good camera control in aid for the survey of building envelopes. Additionally, the UAV application should also be inexpensive. The above considerations (confined operation area, need for hovering, ease of use, and cost limitations) imply that only a multirotor-type UAV is suitable for our application. Table 3 provides the specifications of some of the UAVs that could be used in this study, as their costs fitted the research budget, and they are accompanied by gimbals for image stabilization. In Table 3, "Res" is the resolution of the UAVs' built-in camera, "Flt.Time" is the flight time, "S" is the peak speed, "R" is the operational range, "M" is the mass, and "C" is the battery capacity. Multirotor UAVs typically support small payloads; however, all the models listed in the table are capable of dealing with the lightweight STC, along with the weight of an average smartphone. The total weight would be close to 200 g.

Test flights were planned to test the battery life of the low-cost drones for the survey of a building. As the drone

Thermal Camera	Operational Diameter						
Name	0.5 m		2 m		5 m		
	A [m ²]	2 APP [mm] <i>p</i>	A [m ²]	2 APP [cm ²] <i>p</i>	A [m ²]	2 APP [cm ²] <i>p</i>	
AMG8833	0.32	5000	5.12	800	32	5000	
HT-02 (handheld)	0.03	8.3	0.48	1.3	3	8.3	
Seek thermal	0.10	3.1	1.6	0.5	10	3.1	
FLIR Lepton 3 (chip)	0.38	19	6.08	3.16	38	19	
FLIR 1	0.16	33	2.56	5.3	16	33	
FLIR 1 Pro	0.16	8.3	2.56	1.3	16	8.3	
FLIR DUO	0.17	8.9	2.72	1.4	17	8.9	
Yuneec Typhoon	2.46	9.7	39.36	15	246	9.7	
FLIR VUE	0.04	0.4	0.64	7.44	4	0.4	
Zenmuse XT	0.69	2	11.04	0.33	69	2	

Table 3 Specifications of possible UAVs for the IR—UAV setup.							
Name	Price	Res	R (m)	Flt.Time (min)	S (kph)	M (g)	C (mAh)
DJI Phantom	5000	4000 × 3000	1000	25	56	1216	4480
DJI Spark	6000	3968×2976	100	16	36	300	1480
Up Air One	3800	4896×3264	1000	19	50	1350	5400
Parrot AR Drone	3505	1280 × 720	45	12	18	1800	1000

with gimbal and thermal camera (Table 3) could not be acquired, an available low-cost drone was used and weighed to account for the addition of the STC, a smartphone, and gimbal. The Parrot AR. Drone2.0 (Elite Edition) was chosen for the test flights. The protocol developed by the University of Twente (A.G. Enthrop, A. Vasenev, 2017) was followed in choosing the flight paths.

A building within the university premises (Building 1) was chosen for the simulated survey. The building is a threestory structure, with two tall trees positioned on the North-North Westerly side. The flight plan required the drone to hover and capture images at 2 m away from the building and to be always flying perpendicular to the area of interest. The test was planned to simulate the image-taking process of corners, vents, and roof lining.

The drone was fully charged following the manufacturer's protocol, and the survey flight paths were run (Fig. 2). A successful operation meant that we could utilize the onboard microcontroller to trigger an image capture from the IR camera. A pause of 5 s was used for the points in flight, and the images were to be captured to account for the time that lapsed for capturing an image. The survey was completed in 16 min and 58 s, with over two charges of the battery. The original time planning was 14 min for imaging, 2 min and 39 s for flight, and 30 s as buffer.

We determined that a low-cost UAV could handle the requirements of a survey flight; that is, by using the UAV mounted with IR camera and accessories. However, the list of UAVs presented in this study was not exhaustive, and similar options are always available, even the ones specifically available in certain regions. If the user operating the UAV has sufficient experience with a certain model and is aware of the limitations of the UAV, then efficient survey and savings in terms of time and money can be achieved. In terms of legal restrictions, UAVs to be operated beyond 50 m need approval from the South African Civil Aviation Authority, as stipulated in the South African Civil Aviation Act (UAV).

2.4. Testing the performance of the STC

The steps taken to test the performance of the STC are described briefly in this section, while a more detailed explanation of the setup will be reserved in the Results section. This slightly nonconventional arrangement aims to improve the readability of the paper.

2.4.1. Temperature accuracy

An important aspect of IR thermography-based analysis is the emissivity of the surfaces being analyzed (Avdelidis and







Fig. 2 Images of Building 1, with sample portions of the UAV flight path marked by white lines. (a) Flight paths on a façade. (b) Flight path around the building marked on an aerial view (©Google Maps). The red dot represents one of the staging points on the ground. The blue cross represents a secondary landing site that was kept ready in case of unplanned landing. (c) Flight path along a roof-wall edge.

Moropoulou, 2003). Given that small IR devices, such as Seek Thermal, have auto-emissivity features, the temperature to be measured by the STC should also be validated. The validation is also an important element in the post-processing of images as a means of further extracting research information, as unreliable temperature readings may limit the confounding factors.

2.4.2. Detection of thermal leakages

The aim of this test is to determine a simulated envelope with thermal leakages. A thermal leakage may be caused by numerous reasons, such as structural damage, improper insulation, thermal bridges, damaged insulation, and water retention. On a thermal image, a leakage manifests as an area with a notably different temperature versus its surroundings. According to Balaras and Argiriou (2002), a wide range of temperature difference may mean a variety of seriousness levels of a problem. A 10 K difference is a minor problem that may be handled until the next regular maintenance. However, temperature differences exceeding 30 K imply a serious problem requiring immediate attention, and the issue needs to handled and thoroughly examined in relation to the neighboring area and the system components.

2.4.3. Estimation of leakage area

Thermography, especially when using a consumer-grade device, has limitations in terms of the detection of leakages and the estimation of the seriousness of the leakages. Hence, we explored the possibility of developing an algorithm that could estimate the area of a thermal anomaly (e.g., a leakage) within $\approx 10\%$ error.

Here, the area detection of images involved the use of segmentation algorithms. Specific areas in the images were calculated by counting the number of pixels inside the area. The APP information for the STC, as shown in Table 2, was used to calculate the areas of interest. Before the calculation, a range of simple validation exercises were undertaken to ensure that the specifications given in the datasheets were correct. We were able to verify that the APPs were the same for all pixels as long as the area of interest was maintained within the viewing angle provided by the STC's specifications.

Image segmentation refers to the partitioning of an image into particular parts that are of interest to an application given their similarities in features or properties. The major application fields using image segmentation include medical imaging, content-based image retrieval,

and automatic control systems. Multiple image segmentation techniques can be used to analyze and extract particular information from digital images. These methods can also help improve the quality of images. Image segmentation can be classified into three basic approaches (hybrid, structural, and stochastic; Fig. 3), with each of these approaches entailing a number of subtypes (Anjna and Er, 2017).

As data from the images need to be extracted, the current work explored the following four types of techniques: histogram optimization (with global thresholding) (Sci-Kit Image Development Team), adaptive thresholding (Dwayne Phillips, 1993; Lee et al., 1990), edge-based segmentation (Canny, 1986), and region-based segmentation (Mueller et al., 2004) by using the Canny edge detector.

For the detailed discussion on the different segmentation algorithms, refer to the reviews of Anjna and Er (2017) and Jain (1989). Due to the limited dataset in this work, we only investigated stochastic segmentation algorithms (Fig. 3). After attempting to use the different algorithms, we found the region-based segmentation to be the most suitable for our work, which was somewhat expected. The current study deals with uncertain boundaries for the areas of interest in the thermal image, and edge- and threshold-based methods seemed unsuitable. For example, an edge of an object is sought, and this edge is likely well defined physically. In such scenarios, edge- and threshold-based algorithms can be used in optical image segmentation. However, in our case, the boundary of areas of interests in the thermal image are not well-defined lines.

Our segmentation algorithm required a threshold input. Moreover, we attempted to automate the image segmentation. However, this attempt was unsuccessful in identifying the leakage area. The automatic segmentation did not work for images taken at distances exceeding 2750 mm. Even for images taken at a short distance, we observed issues related to the identification of leakages' shapes and areas and the appearance of image noise. The development of an automated segmentation algorithm will require further work, particularly a comprehensive understanding of the actual camera dynamics in relation to the cost function.

2.4.4. Examination of building envelopes

Building codes have evolved with time, and complex envelope insulation has been continually recommended as a straightforward method for saving building energy consumption. This evolution of envelope insulation should be

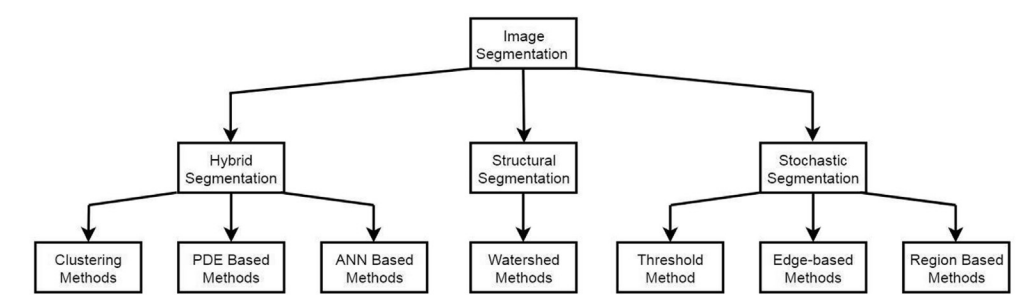


Fig. 3 Image segmentation techniques, adapted from Anjna and Er (2017) PDE refers to partial differential equations and ANN refers to artificial neural networks.

detectable in the IR images of envelopes of two buildings built in different periods. The ability of the STC to take distinguishable images was tested by capturing the thermal images of two new buildings (Buildings 3 and 4) and two old buildings (Buildings 1 and 2). The new and old buildings have at least a 25-year gap between them.

2.5. Data and image analysis

Data analysis and statistical tests were conducted using Python and its SCIPY and Pandas libraries. The normality of the distributions was determined using the Shapiro—Wilk test. The significant differences between normally distributed samples was tested using t-test, whereas the nonnormal samples were tested using Wilcoxon rank test. From the two-sided tests, a one-sided test was also conducted for cases with significant differences. Matplotlib was used for the plotting of graphs, and Sci-Kit libraries were used for the statistical applications and image processing. Tesseract binaries were also used in this work.

The image analysis was conducted using the Jupyter Notebook and several Python libraries. In particular, the SK-image was used to process the images, with the Gaussian filter applied to clear the images of general noise. Then, the Canny filter was used for edge detection, and a binary fill was used to fill the holes. Window filters were also used to clean the images after they were processed. The code used in this work, which can be accessed from https://github.com/NaadirV, has been provided to the research community and can be used as basis for exploring low-cost IR cameras for building surveys.

3. Results and discussions

This section provides the results of the experiments and the tasks involved in image processing. The implications of the results are also discussed in this section, while the limitations of the study will be presented in the Conclusion.

3.1. Temperature accuracy

The accuracy level of the IR camera was gauged by comparing its reading against that of a mercury thermometer. The following temperature/situations were chosen for measurement: ice, boiling water, water allowed to stand at room temperature, and a corner of a PC monitor. According to the datasheet provided by SEEK, the thermal accuracy of the STC is 0.5 °C, which was within the range of temperatures measured for the validation tests. The camera was placed 0.15 m away from the targets except for the PC monitor test, in which the camera was placed 0.25 m away to capture the PC screen in the FOV of the camera.

Wilcoxon rank test was conducted for each of the cases mentioned above (ice, boiling water, water allowed to stand at room temperature, and a corner of a PC monitor) to compare the IR camera and thermometer readings. The null hypothesis could not be rejected for the ice test, the hot water test, and the PC screen test. The difference between the medians of the thermometer and the STC measurements were thus not statistically significant. By contrast, the difference was significant between the

thermometer and STC measurements for the room temperature test ($Z_{calc} < Z_{standard}, -10.52 < -1.96$).

Four hundred temperature measurements were recorded. Only 19 of the IR readings from the STC were within $\pm 0.5~^{\circ}\text{C}$ relative to the thermometer readings. Fig. 4 shows the IR camera readings versus the thermometer readings, in which the high overlap is presented by the concentrated blue labels in the plot.

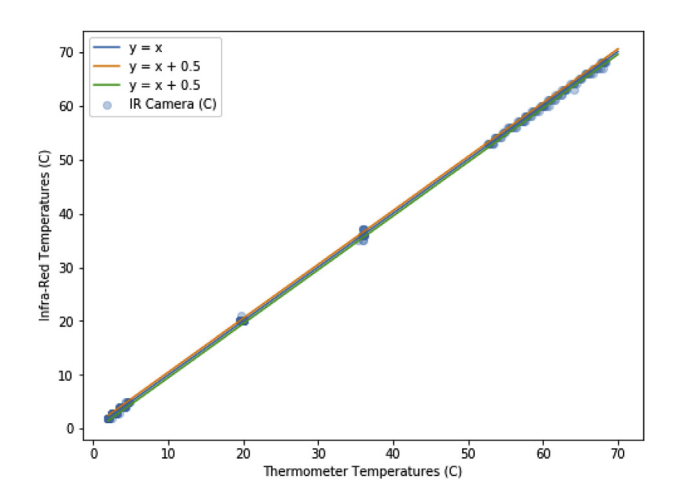


Fig. 4 Scatter plot of the overlay between the thermometer and IR camera data.



Fig. 5 Optical image of a tile with 16, 14, and 10 mm-diameter holes as an example of the setup.

Only few mismatches are shown in Fig. 4, which may have been caused by the slight misalignment in pointing the IR camera versus the position of the thermometer; however, majority of the aligned cases imply that the STC's measured temperature values are reliable.

3.2. Detection of thermal leakages

In ideal scenarios, an IR inspection system should be able to detect even the smallest leakage. Here, six 5 mm-thick holes were drilled into two glazed ceramic tiles at three holes for each tile (see Fig. 5). These holes ranged in the diameters of 3, 5, and 8 mm for Tile 1 and 10, 14, and 16 mm for Tile 2. The smallest hole diameter was chosen on the basis of the smallest drill bit available. A tungsten lightbulb was placed inside a box and used as the heat source. The sides of the box were sealed with silicone to be able to maximize the heat exiting through the holes.

The images were then taken at the distances of 750 and 1750 mm for Tile 1 and 2750 and 3750 mm for Tile 2. Most cameras affixed on drones can focus on an object as close as 500 mm (DroneZon). The closest imaging distance of 750 mm was selected was to ensure that a common drone could focus on the envelope while still not bumping into it, presuming that the control was not optimal. The longer

distances were set in four steps at 1 m each starting from the shortest distance.

The images of tiles placed in front of the heat source were also taken using the Testo 882 IR camera (resolution: 320×240 pixels: cost \approx R85.000)) and then compared with the images from the STC (resolution: 206×156 pixels). The Testo camera has a feature of combining optical images (resolution: 640×480 pixels) and thermal images to achieve high-level details. As previously mentioned, our hypothesis is that lower-resolution images can be postprocessed using simple digital image processing techniques to yield the detection of leakages with sizes similar to those images generated by higher-resolution expensive devices. The STC image was therefore processed with image segmentation techniques and cleaned of excess noise by using iterative window filters. On the basis of the algorithms discussed in Section 2.4.3, we found through quantitative testing that region-based segmentation, together with window filtering, was the best method for our particular investigation.

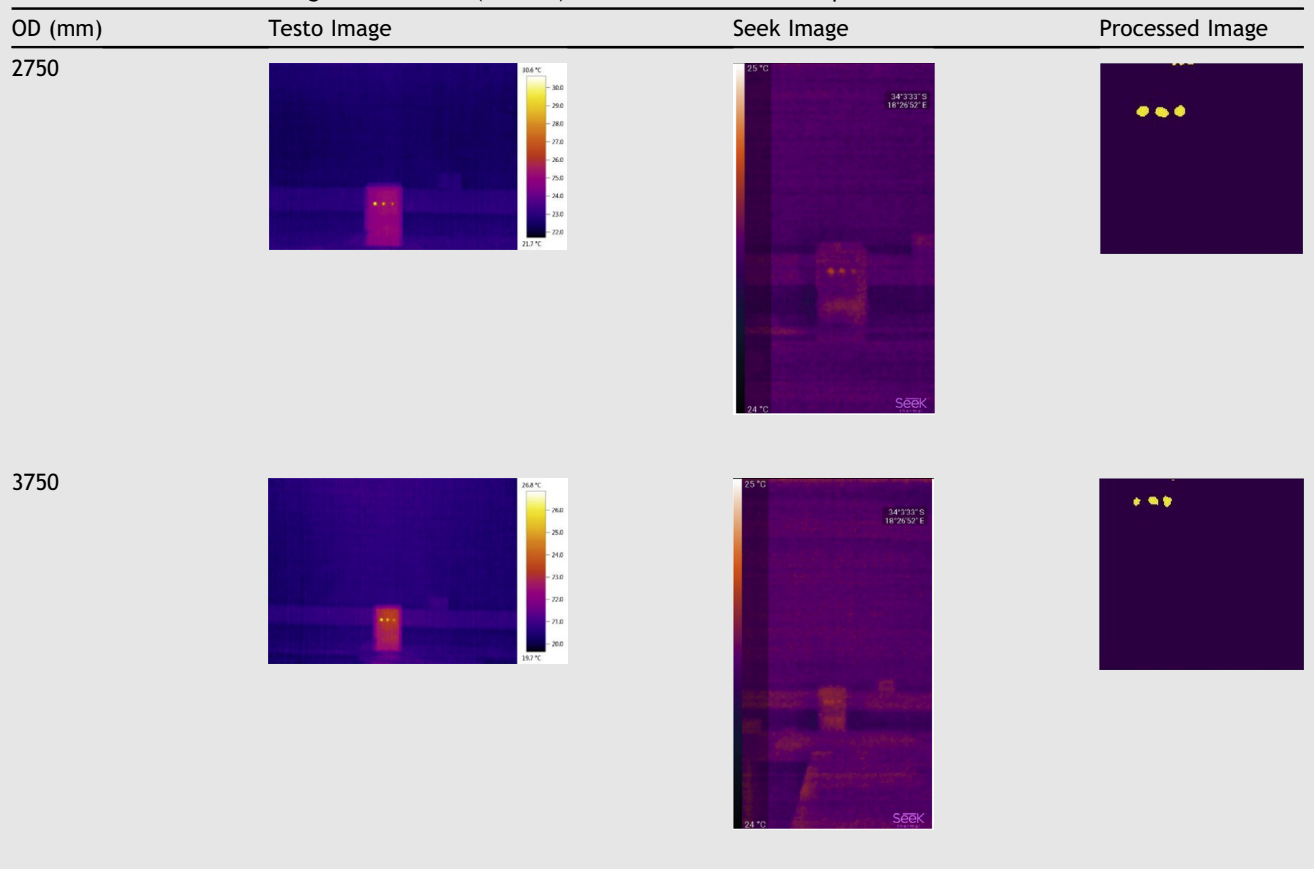
Tables 4 and 5 present the results of the images captured by the abovementioned two cameras given a set of size anomalies (holes). In addition to the original image captured by the STC, we also show the images after post-processing. A number of the processed images appear to

Table 4 Thermal images captured by Testo and Seek Thermal cameras at various distances from a tile with 3, 5, and 8 mm-diameter holes.

DD (mm) Testo Image Seek Image Processed Image

750

Table 5 Thermal images captured by Testo and Seek Thermal cameras at various distances from a tile with 10, 14, and 16 mm-diameter holes. The following classifications (Table 6) were used to review the performances of the different cameras.



Clearly Visible: Three separate well-defined holes.

Visible: Three holes are shown but are slightly distorted.

Partially visible: Not all holes are well defined or detectable, but there is evidence of one or more anomalies.

Not visible: No visible hole marks.

Good detection: Three well-defined holes shown in the processed image.

Detection: Three holes shown in the processed image, but they have some deformity and/or noise.

Partial detection: Not all holes are well defined or detectable, and there is evidence of anomalies in the processed image.

No detection: No clear evidence of holes in the processed image.

be differently sized, as they have been cropped to remove unnecessary noise from the unfavorable surrounding portions. For the three larger holes, only the images taken at greater distances (2750 and 3750 mm) are presented. For the smaller holes, only the images taken at the shorter distances (750 and 1750 mm) are shown.

Table 6 Qualitative evaluation of the thermal detection of flaws for the tile with 8, 5, and 3 mm holes photographed at 750 and 1750 mm and for the tile with 16, 14, and 10 mm holes photographed at 2750 and 3750 mm.

OD (mm)	Testo	Seek	Processed
750	Clearly Visible	Clearly Visible	Good Detection
1750	Clearly Visible	Clearly Visible	Detection
2750	Clearly Visible	Clearly Visible	Detection
3750	Clearly Visible	Visible	Detection

As shown in Tables 3 and 4, the anomalies at specific distances are visible for both cameras, with the processed images improving the estimation of the flaws' position and outline. Here, the visibility of the flaws was subsequently qualitatively classified.

This work ultimately aims to mount the STC on a UAV for the evaluation of the building envelope. In this scenario, the UAV can fly within 2 m of the surveyed structure. The results obtained from the simulation were promising and even comparable with the expensive Testo camera.

The enclosure that was used to house the incandescent lamp was made from 5 mm wood. During the experiment, the structure heated up and caused additional noise in the image. This drawback will not be observed when typical building envelope elements are examined, as they are thermally much more massive and/or have relatively high thermal insulation. The images of the anomalies in a building envelope may be expected conservatively, that is, they will appear as having much less noisy images.

3.3. Estimation of leakage area

The ability of the STC to estimate the areas of anomalies was tested by creating sample images, particularly by placing pieces of cardboard in front of the heat source. Each piece of cardboard had a laser cut hole. For dimensional accuracy, we set the diameters of the hole as 10, 20, 30, 40, and 60 mm. The images were taken at the distances of 750, 1750, 2750, and 3750 mm.

As mentioned in Section 3.2, after testing different segmentation techniques, we could proceed with region-based segmentation. The region-based segmentation was also applied to the STC IR images for the evaluation of areas of anomalies. Fig. 6 shows the original IR image and the image after region-based segmentation. The segmentation clearly resulted in a flaw boundary with the creation of a uniform background.

The algorithms with a manually fed segmentation threshold preserved the shape much better compared with the shapes shown in the automatic segmentation tests. The area estimation results for the 10 mm hole are shown in Table 7. The results correspond to images taken at distances of up to 2750 mm. At distances further than 2750 mm, the results were consistently erroneous. A number of processed images shown in Table 7 were cropped to remove unwanted captured noise from the surrounding. In particular, for the images taken at further distances, when the FOV captured a larger area, unwanted noise in the image were included. Using a cropped image removed the unnecessary noise from the unfavorable surrounding environments. As the experiment was focused on area detection only, the cropping out of external noise can be regarded within the scope of the study.

Table 8 provides the best-case error in area estimation for the differently sized holes. The smallest error of 1.4% was observed at 750 mm for the 10 mm-hole area estimation of the STC IR image. This achievement rate was impressive but rather unexpected. Moreover, this rate was also the only within the 10% error for the estimation, which was the stated aim of this study.

The error derived from estimating the area of the anomaly generally increases with the distance of the captured image. This finding can be ascribed to the low-resolution image feature of the STC and the relatively small anomaly detected together with the background noise

influencing the gradient of the image. The increase in error can also be explained by the most appropriate cost function for segmentation. However, the cameras' dynamics were not derived in this work.

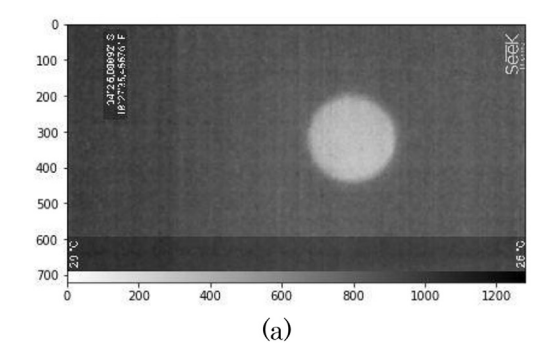
Only one of the area estimates, namely, the tests of the 10 mm-diameter anomaly, that were measured at 750 mm proved to be within the 10% error, as initially targeted. However, the segmentation was successfully applied to the STC's low-resolution images, and the area could be estimated from the processed images. Similar to the case detection of thermal images, the best results for area estimation were also found for images captured at the 750 or 1750 mm distances. This finding implies that the STC can function reasonably well when mounted on the UAV and estimate the size of any damage to the envelope's insulation.

3.4. Examination of building envelopes

The STC was used to obtain the thermal images of a wall from each of the four buildings, namely, two new buildings (Buildings 3 and 4) and two older constructions (Buildings 1 and 2). The images were taken on the same day and with as minimal time gap as possible to avoid drastic changes in the outdoor conditions. The IR images of the indoor and outdoor walls of the same portion of the buildings were captured. The indoor and outdoor air temperatures were also simultaneously measured with a mercury thermometer.

An algorithm was used to post-process the images, and an area weighted average temperature was obtained for the portion of the examined wall. The average value of the pixels was calculated according to a linear model; then, on this basis of the modeling results, the average temperature was calculated for the image. The images were taken in grayscale, as this process could assist in the post-processing. Capturing colored images and simply converting them into grayscale images would lead to avoidable data loss during conversion.

The results of the temperatures measured for the four buildings are summarized in Table 9. In addition, Fig. 7 provides the internal and external wall images of one of the old buildings, while Fig. 8 provides similar images for one of the new buildings. The area weighted average temperatures were computed using similar images.



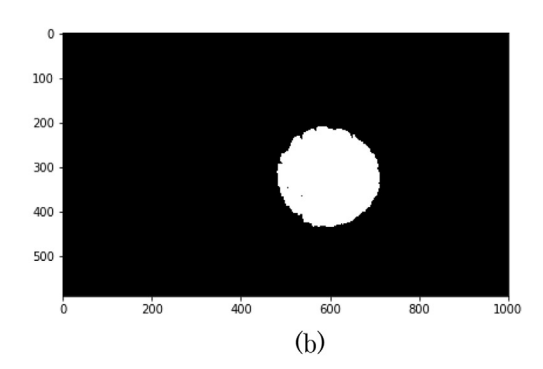


Fig. 6 (a) Original IR image and (b) region-based segmentation applied to the IR image with a 60 mm-diameter hole captured at 750 mm.

diameter anomaly. OD [mm] Seek Image Processed Image Area [mm²] 750 77.43 1750 437.87 2750 782.47

Table 7 Thermal images and processed images captured by the STC at distances of 750, 1750, and 2750 mm for the 10 mm-diameter anomaly.

As shown in Table 9, the wall temperatures calculated using the STC images were able to distinguish between the envelopes of buildings with different levels of insulation in lieu of their different periods of construction. This study was undertaken primarily as a field implementation of the STC's abilities. At the same time, we were able to perform image processing, aimed at determining the area weighted average temperature, in a relatively simple manner for the interpretation of IR images.

A brief overview of extant literature on the subject was previously presented in the Introduction.

Thus far, studies have not focused on the importance of post-processing the IR images. We showed that by using open-source computational tools and algorithms for image processing, the IR images can attain relatively clear

contrasts and render the anomaly detection less difficult. This approach is especially valuable in the use of consumer-grade IR cameras for building surveillance. The image post-processing may be viewed as a branch of the approach in which numerical heat transfer techniques are combined with IR images to achieve a quantitative evaluation of a façade's insulation (Nardi et al., 2014; Lagüela et al., 2012). Through this work, we hope to provide a basis for similar explorations. For our specific situation and dataset, we found that region-based segmentation, with a manually provided threshold level, as the most useful method. Future research seeking other kinds of defects may attain similarly good results by using other segmentation algorithms. Moreover, with much more

Table 8 Best-case error for the area estimation of flaws from the IR images and the corresponding distances of the captured image.

Hole size (mm)	OD (mm)	Error (%)	Diameter estimate (mm)
10	750	-1.4	9.9
20	750	37.9	23.5
30	750	26.6	33.8
40	1750	21.7	44.1
60	1750	-16.4	54.8

Table 9 Results for the wall and air temperatures for the four studied buildings.

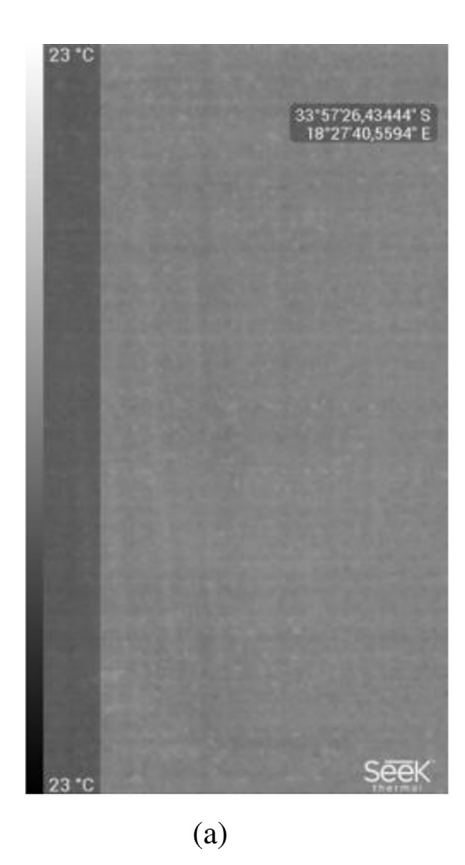
Building	Year of construction	T _{inair} [°C]	T _{inwall} [°C]	T _{outwall} [°C]	T _{outair} [°C]
Building 1	1929	23	23	25	31
Building 2	1966	21	27	32	33
Building 3	2014	22	23	27	31
Building 4	2013	21	25	31	32

thorough information about camera characteristics, we believe that threshold inputs can also be automated.

3.5. Study limitations

The types of thermal camera and drone made available to the researchers as a local consumer were limited due to strict export regulations in the supplier country. Hence, the chosen thermal camera and drone were not necessarily the ideal choice. Logistical considerations, such as postal backlog, fluctuating exchange rates of the South African Rand, and the overall budgetary limitation of R10 000, also hinged us to acquire certain cameras at a time when desirable weather was also considered for running the tests on the IR camera-UAV combination. The accuracy of IR imaging can be affected by a multitude of environmental factors that are beyond our control (Sadineni et al., 2011). A high concentration of particulate matter in the air can attenuate IR transmission. Windy conditions (>5 m/s) and bouts of rain can also pose a problem to UAV flight and the accuracy of IR inspection (O'Grady et al., 2017).

The results discussed above indicate that the limitations should also be considered. First, while the STC yielded highly convincing results, as described in the previous sections, the results would have been better in terms of resolution and with respect to the accuracy derived from the area and detection tests. We suspect that anomalies may be detected at a longer range and with a smaller error. However, the camera we selected was a value-for-money tool offering the best resolution despite the price limitation



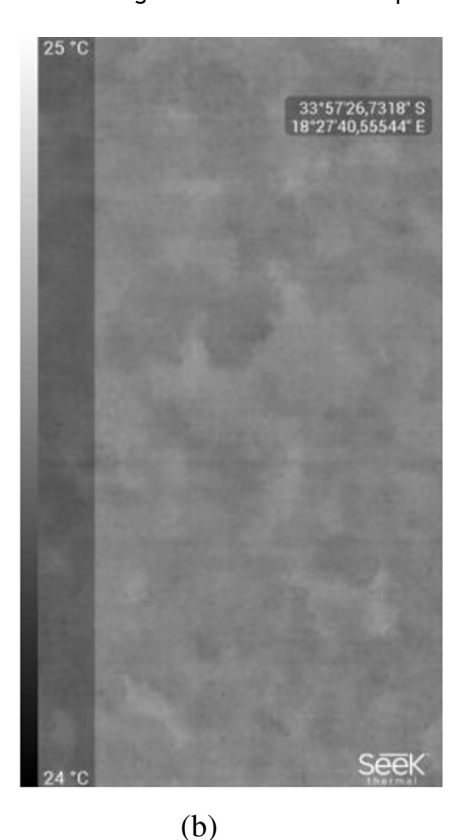


Fig. 7 (a) Internal and (b) external IR images of the wall of Building 1.

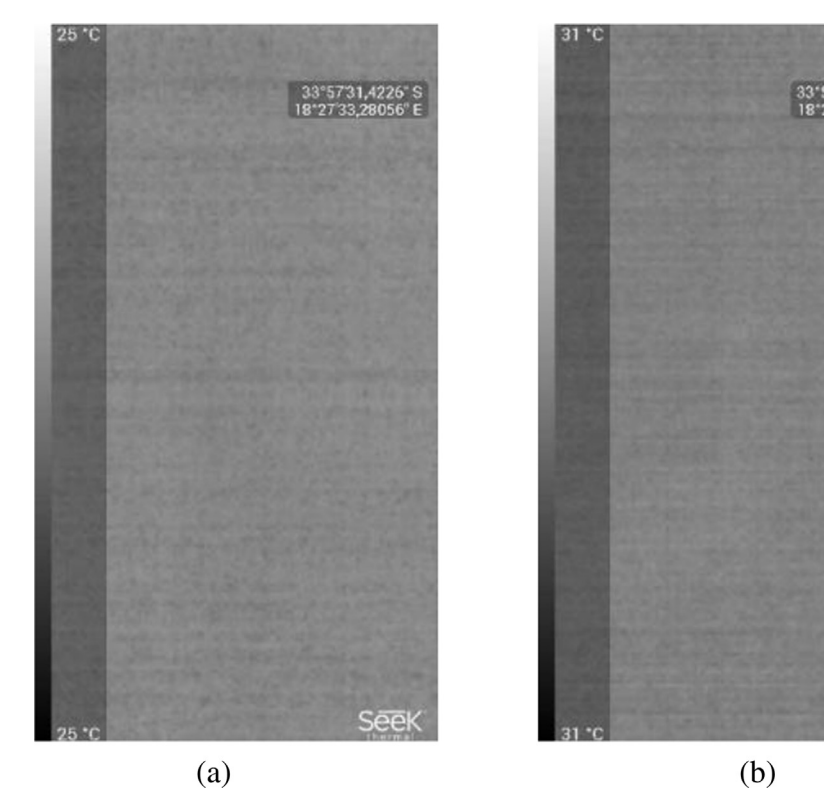


Fig. 8 (a) Internal and (b) external IR images of the wall of Building 4.

but still could be used for anomaly detection as theorized. Future work may contemplate the use of image processing to overlay the thermal image from STC with an optical image, as what is inherently done by costlier camera counterparts, to improve details perceived in the image.

Second, the camera changes the color scale with respect to the environment in which it is used. The use of such a camera is suitable for environments with large temperature differences, as the camera will need to show all the different temperature values with a fixed number of colors. Although this feature is great as a camera feature, it makes the algorithm setup particularly difficult to use because the scales representing certain intensities also need to be changed. Third, we suspect that the relationships among FOV, distance, and pixel size are not completely understood with respect to how the camera registers an image. We also suspect that this issue is one of the reasons for the errors in the area estimation.

4. Conclusion

The current study documents the steps undertaken in analyzing the performance of STC as a low-cost IR camera for building inspection. The device, despite its low cost, was reasonably accurate at measuring the temperature of objects, both in laboratory-controlled conditions and in the field. Although the image quality from the Seek Thermal was determined to be poorer than those of expensive IR cameras, the resulting images captured at the distance of 750 mm from the target provided comparable details. Furthermore, with minimal post-processing of images and the use of open-source libraries and computing

environment, the ability of the STC to detect small anomalies can be easily enhanced. Even at a distance of nearly 2 m from the target, the post-processed images can spot anomalies as small as 3 mm in diameter. Similarly, within distances of ~1.5 m, the STC's IR images can be post-processed to provide a reasonable estimate of areas with thermal anomalies. The measurements of actual building walls showed that the images captured by the STC can be used to distinguish the insulation levels of different building envelopes with ease.

With these realizations, the STC proves to be a reasonably effective IR camera, given its affordable price and the absence of export regulations. At the same time, the STC offers a simple user interface, and its small size is suitable as a payload for inexpensive drones. We hope that this work will provide a suitable basis for other works that intend to utilize low-cost thermography and ultimately lead to the widespread use of these techniques in building surveys.

Acknowledgement

The second author was supported by the Republic of Singapore's National Research Foundation, through the Singapore—Berkeley Building Efficiency and Sustainability in the Tropics Program, which is an undertaking of the Berkeley Education Alliance for Research in Singapore.

References

Anjna, E.A., Er, R.K., 2017. Review of image segmentation technique. Int. J. Adv. Res. Comput. Sci. 8 (4).

Athalye, R.A., Sivaraman, D., Elliott, D.B., Liu, B., Bartlett, R., 2016. Impacts of model building energy codes. Tech. Rep. Pacific Northwest National Lab., Richland, WA.

- Avdelidis, N., Moropoulou, A., 2003. Emissivity considerations in building thermography. Energy Build. 35 (7), 663–667.
- Balaras, C., Argiriou, A., 2002. Infrared thermography for building diagnostics. Energy Build. 34 (2), 171–183.
- Barreira, E., Almeida, R.M., Moreira, M., 2017. An infrared thermography passive approach to assess the effect of leakage points in buildings. Energy Build. 140, 224–235.
- Canny, J., 1986. A computational approach to edge detection. IEEE Trans. Pattern Anal. Mach. Intell. 6, 679—698.
- Choi, G.S., Kim, K.W., Kang, J.S., Lee, S.E., 2007. Evaluation on thermal performance combined with measurement and simulation for development of on-site evaluation method. SAVE Proc.: Building Simulation 2007 175—182.
- Cox, S., 2016. Building Energy Codes: Policy Overview and Good Practices. Tech. Rep. National Renewable Energy Laboratory (NREL), Golden, CO (United States).
- De Wilde, P., 2014. The gap between predicted and measured energy performance of buildings: a framework for investigation. Autom. ConStruct. 41, 40–49.
- Enthrop, A.G., Vasenev, A., 2017. Infrared drones in the construction industry: designing a protocol for building thermography procedures. Energy Procedia 132, 63—68.
- Ferrarini, G., Bison, P., Bortolin, A., Cadelano, G., 2016. Thermal response measurement of building insulating materials by infrared thermography. Energy Build. 133, 559–564.
- Fox, M., Goodhew, S., De Wilde, P., 2016. Building defect detection: external versus internal thermography. Build. Environ. 105, 317–331.
- Gillott, M., Loveday, D.L., White, J., Wood, C., Chmutina, K., Vadodaria, K., 2016. Im- proving the airtightness in an existing UK dwelling: the challenges, the measures and their effectiveness. Build. Environ. 95, 227–239.
- Goodhew, J., Goodhew, S., Auburn, T., De Wilde, P., Pahl, S., 2009. A preliminary investi- gation of the potential for thermographic images to influence householders understanding of home energy consumption. In: Procs 25th Annual ARCOM Conference. Citeseer, pp. 7–9.
- Jain, A.K., 1989. Fundamentals of Digital Image Processing. Prentice Hall, Englewood Cliffs, NJ.
- Kim, J.-J., Moon, J.W., 2009. Impact of insulation on building energy consumption. In: Build- Ing Simulation, vol. 2009. Citeseer, pp. 674–680.
- Kirimtat, A., Krejcar, O., 2018. A review of infrared thermography for the investigation of building envelopes: advances and prospects. Energy Build. 176, 390—406.
- LaFrance, M., et al., 2013. Technology roadmap: energy efficient building envelopes. In: Energy Technol. Pol. Div. IEA.

Lagüela, S., Armesto, J., Arias, P., Herráez, J., 2012. Automation of thermographic 3d mod- elling through image fusion and image matching techniques. Autom. ConStruct. 27, 24—31.

- Lee, S.U., Chung, S.Y., Park, R.H., 1990. A comparative performance study of several global thresholding techniques for segmentation. Comput. Vis. Graph Image Process 52 (2), 171–190.
- Liu, W., Zhao, X., Chen, Q., 2018. A novel method for measuring air infiltration rate in buildings. Energy Build. 168, 309—318.
- Mueller, M., Segl, K., Kaufmann, H., 2004. Edge-and region-based segmentation technique for the extraction of large, manmade objects in high-resolution satellite imagery. Pattern Recogn. 37 (8), 1619–1628.
- Nardi, I., Sfarra, S., Ambrosini, D., 2014. Quantitative thermography for the estimation of the u-value: state of the art and a case study. In: Journal of Physics: Conference Series, 547. IOP Publishing, pp. 12—16.
- O'Grady, M., Lechowska, A.A., Harte, A.M., 2017. Infrared thermography technique as an in-situ method of assessing heat loss through thermal bridging. Energy Build. 135, 20—32.
- O'Grady, M., Lechowska, A.A., Harte, A.M., 2018. Application of infrared thermography technique to the thermal assessment of multiple thermal bridges and windows. Energy Build. 168, 347–362.
- Phillips, D., 1993. Image processing, Part 9: histogram-based image segmentation. C Users J. 11 (2), 63–88.
- Plowright, A., 2016. Using thermal cameras to promote energy efficiency in buildings. Available online at: https://sustain.ubc.ca. (Accessed 22 April 2020).
- Sadineni, S.B., Madala, S., Boehm, R.F., 2011. Passive building energy savings: a review of building envelope components. Renew. Sustain. Energy Rev. 15 (8), 3617—3631.
- Sfarra, S., Cicone, A., Yousefi, B., Ibarra-Castanedo, C., Perilli, S., Maldague, X., 2019. Im- proving the detection of thermal bridges in buildings via on-site infrared thermography: the potentialities of innovative mathematical tools. Energy Build. 182, 159—171.
- Sun, X., Brown, M.A., Cox, M., Jackson, R., 2016. Mandating better buildings: a global review of building codes and prospects for improvement in the United States. Wiley Interdisciplinary Reviews: Energy Environ. 5 (2), 188–215.
- Tejedor, B., Casals, M., Gangolells, M., Roca, X., 2017. Quantitative internal infrared ther-mography for determining in-situ thermal behaviour of fa,cades. Energy Build. 151, 187–197.
- UNEP, 2012. Building Design and Construction: Forging Resource Efficiency and Sustainable Development. June 2012.
- Young, R., Hayes, S., Kelly, M., Vaidyanathan, S., Kwatra, S., Cluett, R., Herndon, G., 2014. The 2014 international energy efficiency scorecard. In: American Council for an Energy- Efficient Economy. USA.